electronics

Article

Tuning Bolometric Parameters of Sierpinski Fractal Antenna-Coupled Uncracked/Cracked SWCNT Films by Thermoelectric Characterization at UHF Frequencies

Gustavo Vera-Reveles [1], José Vulfrano González-Fernández [1], Juan Francisco Castillo-León [1], Francisco Javier González [2,3], Ramón Díaz de León-Zapata [1], Ariel Benjamín de la Rosa-Zapata [1], Norma Orocio-Castro [1] and Jorge Simón [4,*]

[1] Departamento de Electrica, Electronica, Mecatronica, Tecnologico Nacional de Mexico/Instituto Tecnológico de San Luis Potosí, San Luis Potosi 78437, Mexico; gustavo.vr@slp.tecnm.mx (G.V.-R.); fanogf@gmail.com (J.V.G.-F.); juan.cl@slp.tecnm.mx (J.F.C.-L.); ramon.dd@slp.tecnm.mx (R.D.d.L.-Z.); ariel.dl@slp.tecnm.mx (A.B.d.l.R.-Z.); norma.oc@slp.tecnm.mx (N.O.-C.)
[2] Centro de Ciencia y Tecnologia de Terahertz, Universidad Autonoma de San Luis Potosi, San Luis Potosi 78000, Mexico; javier.gonzalez@uaslp.mx
[3] Laboratorio Nacional de Ciencia y Tecnologia de Terahertz, Universidad Autonoma de San Luis Potosi, San Luis Potosi 78000, Mexico
[4] Catedras CONACYT, Centro de Investigacion, Innovacion y Desarrollo en Telecomunicaciones, Unidad Academica de Ingenieria Electrica, Universidad Autonoma de Zacatecas, Zacatecas 98000, Mexico
* Correspondence: jorge.rodriguez@uaz.edu.mx

Citation: Vera-Reveles, G.; González-Fernández, J.V.; Castillo-León, J.F.; González, F.J.; Díaz de León-Zapata, R.; de la Rosa-Zapata, A.B.; Orocio-Castro, N.; Simón, J. Tuning Bolometric Parameters of Sierpinski Fractal Antenna-Coupled Uncracked/Cracked SWCNT Films by Thermoelectric Characterization at UHF Frequencies. *Electronics* **2022**, *11*, 1665. https://doi.org/10.3390/electronics11111665

Academic Editor: Antonio Di Bartolomeo

Received: 14 April 2022
Accepted: 21 May 2022
Published: 24 May 2022

Abstract: In this work, the bolometric parameters of Sierpinski fractal antenna-coupled SWCNT semi-metallic films are obtained by thermoelectric characterization, this in order to find out the performance as bolometer. The method was based on an experimental setup considering a line-of-sight wireless link between two identical planar fractal antennas, infrared thermography, and electrical resistance measurements. The experimental setup considered the antennas resonant frequencies. Both the transmitting and receiving antenna were third-iteration Sierpinski fractal dipoles designed to work at UHF frequencies. Films made either of cracked or uncracked SWCNT films were each separately coupled to the receiving fractal antenna. Measurements showed that the receiving antenna that was impinged with radiation at UHF frequencies coming from the transmitting antenna, experienced as it was expected an induction of electric current, the induced current flowed through the film producing a temperature change, which in turn caused changes in the radiated heat of the film, as well as changes in the electrical resistance known as Temperature Coefficient of Resistance TCR. The maximum value of TCR for uncracked SWCNT films was $-3.6\%\mathrm{K}^{-1}$, higher than the one observed for cracked SWCNT films which exhibited a maximum value of $-1.46\%\mathrm{K}^{-1}$. Measurements for conversion of incident radiation to electrical signals known as the Voltage Responsivity $\Re_v$, exhibited values of 9.4 mV/W and 1.4 mV/W for uncracked SWCNT films and cracked SWCNT films, respectively.

Keywords: bolometric parameters; thermoelectric characterization; uncracked and cracked SWCNT; Sierpinski fractal antenna; UHF frequencies

1. Introduction

Carbon nanotubes (CNT) have been used as detectors for different applications, including microwave and terahertz detection [1–7]. Bolometers have been especially applied to early detection of biological abnormalities in humans and animals as well as in living tissue samples, space radiometry, optical communication, thermal imaging for military applications, or for non-contact temperature measurements among others [8].

One of the most common thermal detectors is the bolometer. The term 'bolometer' is a composite word with a Greek origin, formed by *bole* (beam, ray) and *metron* (meter, measure) [9]. In practice, it is a temperature-sensitive electrical resistor. As a consequence, a significant change in the electrical resistance occurs when the detector is heated by incident radiation measured by an external electrical circuit [10,11]. The electrical resistance of the film is controlled while the radiation is absorbed and its temperature increases. If the film is a semiconductor, the resistance decreases as the temperature rises, hence, it is said to have a negative temperature coefficient of resistance [12]. The temperature coefficient of resistance is measured as a percent change of resistance per degree Kelvin ($\%K^{-1}$). The TCR values of materials used as bolometric detectors, such as vanadium oxide (VOx) or amorphous silicon (a-Si), are around -4 and –2.5$\%K^{-1}$ respectively [13–15]. Smaller bolometers heat up faster which speeds up their frequency response [16] and if they are coupled to an antennas it is possible to tune the frequency and the polarization of the incoming radiation, as well as take advantage of the capture region provided by the area occupied by the antenna [17].

Previous investigations reported that a holey carbon nanotube network was designed with the vision of improving the TCR for ultra-fast broadband bolometers. The obtained films demonstrate a high TCR over a wide temperature range, up to $-2.8\%K^{-1}$, however, those values were measured at temperatures much lower than room temperature, i.e., at liquid nitrogen temperature [18]. On the other hand, reported work indicates that a radio frequency bolometer was implemented using a thermistor fabricated from a carbon nanotube thin film deposited on a sapphire substrate, with the thermistor held at a temperature of 15 °C. The bolometer sensitivity at 915 MHz was found to be 0.36 mV/mW, however these values of data points were collected while sweeping the bias up from 1 to 30 V [19].

Regarding antennas and carbon nanotubes, there have been many developments of antennas or other electromagnetic devices made by carbon nanotubes for diverse purposes such as a multiband wireless antenna working at 900 MHz, 2.4 GHz, and 5.5 GHz [20], or data transmission lines for ultrawideband medical wireless body area networks [21,22], while in our study the multiband antenna is made of cooper on a dielectric substrate, being a SWCNT film coupled between the terminals of the feed.

In this work, the thermoelectric performance was focused on two key figures of merit in bolometric detectors: Temperature Coefficient of Resistance (TCR) and Voltage Responsivity ($\Re_v$). The study was conducted for cracked and uncracked films of single-walled carbon nanotubes (SWCNT) coupled to a receiving third-iteration Sierpinski fractal dipole antenna working at UHF frequencies. In addition, the heat radiated in each of the samples was calculated and thermoelectric characterizations were performed at room temperature and atmospheric pressure.

This article is organized as follows: Section 2 shows a brief description regarding single-walled carbon nanotube (SWCNT) films used as bolometers. It also includes the antenna design, i.e., the fractal shape, dimensions, resonance frequencies corresponding to each of the fractal iterations, the coupling of bolometers to the receiving antenna, and the experimental setup used to perform the measurement of thermoelectric characterization. In Section 3, the bolometric performance of both uncracked and cracked films is shown as a result related to electrical resistance, the temperature, and incident radiation frequency. In addition, an analysis of conversion of incident radiation into electrical signals and radiated heat in each of the samples is performed. Finally, the conclusions are provided in Section 4.

2. Materials and Methods

2.1. SWCNT Films as Bolometers

The detailed preparation and device fabrication of each of the samples are described in [23–26], briefly, both films of nanotubes there was the same density of deposit, but different drying conditions.

The ink dispersion is deposited onto a doped polycrystalline-silicon substrate capped with a silicon oxide surface in an oven at 80 °C for 48 h, for a relative humidity lower than 20% is due to that, after deposition the ink is then cured under a 60 °C lamp for several hours to remove any remaining moisture. This is possible to observe that the continuity in the SWCNT film on the silicon substrate is highly reduced, the composite formed exhibits micron-scale cracks, as well as in the dried composite contain highly aligned SWNTs suspended above the substrate perpendicular to the crack. (Figure 1b).

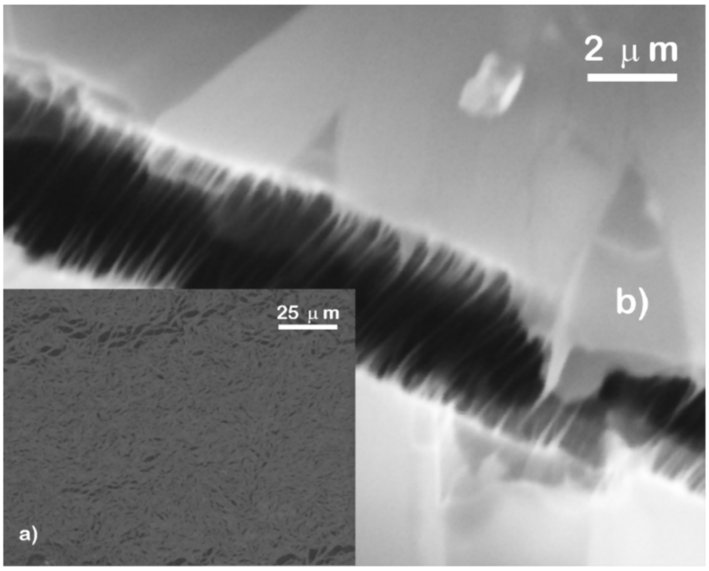

Figure 1. SEM images for (**a**) high continuity on SWCNT uncracked film and (**b**) low continuity on SWCNT cracked film.

In contrast, when the humidity is high and the drying occurs slower, very few if any cracks are observed, relative humidity higher than 80% (Figure 1a), the deposit shows a SWCNT film with high continuity and alignment. The film thickness was 2 μm; SEM images (Scanning Electron Microscope) were taken using FEC-SEM model INSPECT RF50.

2.2. The Antenna-Coupled SWCNT Bolometers

The antenna that was coupled to SWCNT films is a planar dipole formed by two equilateral Sierpinski fractal triangles (10 cm long and 1 cm apart). Its fabrication was based on third-iteration level [27,28] and it was fabricated of a copper thin film (FR2 paper resin copper clad laminate) using conventional printed circuit board (PCB) techniques. The SWCNT thin films deposited on a 1 cm × 0.4 cm doped polycrystalline-silicon substrate were fixed at the antenna feed gap (between the dipole arms) and were electrically coupled to two silver stripes (3 mm long, 1 mm wide and 8 mm apart) deposited atop the SWCNT using a conductive silver ink and anchoring copper wires to create electrical contacts to allow thermal and electrical characterization. The fractal antenna which was coupled to the SWCNT bolometers, is wideband and it itself has 4 well-defined theoretical resonant frequencies values for iterations from 0 to 3 [29–33]. To confirm the 4 frequency bands at which the antenna operates, by measurements a graph corresponding to parameter S_{11} in dB was obtained by using an N5222A vector network analyzer (VNA) from Keysight Technologies® (Santa Rosa, CA, USA) and considering 50 Ω 1-port SOLT calibration. The graph that was taken directly from the measurement instrument includes markers pointing the resonances (minimum values within each of the 4 bands), i.e., the frequencies at which the antenna has better impedance matching with the transmission line. Figure 2 shows the resonance frequencies which are 0.331, 1.644, 3.006 and 8.418 GHz corresponding to iterations 0 to 3. It is worth mentioning that in Section 2.3 a frequency of 554.5 MHz belonging to the first band of the fractal antenna will be used to perform the characterization at which the antenna itself has an S_{11}(dB) of at least −7.16 dB [34]. The characterization at 554.5 MHz was performed as a proof of concept that verifies that an electromagnetic wave at UHF frequencies incident on the antenna induces a current in the antenna arms that circulates through the bolometer. The rest of the resonant bands are available for other future applications.

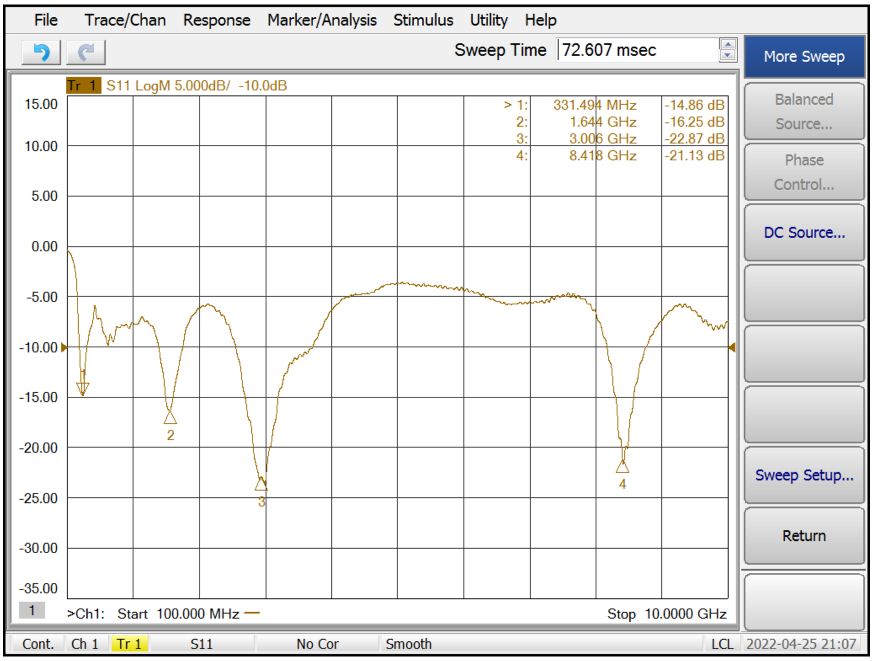

Figure 2. Parameter S_{11} in dB corresponding to the third–iteration Sierpinski fractal dipole.

2.3. Characterization Based on a Line-of-Sight UHF Link

The radiation source that was used consisted of a transmitting third-iteration Sierpinski fractal antenna (TA) which had the same dimensions, polarization, and shape as the receiving one, i.e., the antenna under test (AUT). The TA was fed by a radiofrequency generator (RFG), that works from 554.5 MHz to 678.5 MHz (UHF frequencies) and it is able to supply a 1.5 W output. The RFG was connected to the TA through a 75 Ω coaxial transmission line whose length was 1 m. The RFG was chosen for the thermoelectric characterization since bolometric detectors coupled to the AUT are wavelength independent [35] and are able to work at UHF frequencies. The AUT was placed at a distance of 0.25 m from the TA which ensured the position in the far-field region for the entire frequency sweep from 554.5 MHz to 678.5 MHz that was carried out existing a line-of-sight link [36].

Thermal and electrical properties of the AUT-coupled SWCNT bolometers were obtained by using a high-resolution infrared (IR) camera with a thermal sensitivity higher than 50 mK and a 240 × 256 focal plane array of VOx microbolometers (FLIR T400, FLIR Systems Inc., Wilsonville, OR, USA) in order to measure temperature, and a Fluke 289 digital multimeter with data logging capabilities to measure electrical resistance, respectively. Thermoelectric measurements for the AUT-coupled SWCNT bolometers were performed by means of taking a total of 10 IR thermographs of them, of which only the first one was taken without receiving radiation from de TA connected to the RFG, while for the subsequent IR images a sweep in the RFG feeding the TA including 9 frequencies between 0-th and 1st AUT iterations was performed. Electrical resistance measurements were also performed for each of the aforementioned frequencies. These thermoelectric measurements were performed placing the IR camera at a distance of 0.6 m facing the AUT-coupled SWCNT bolometers in order to obtain a numerical value of the mean temperature for the different thermographs. Figure 3 shows the experimental setup while in Figure 4 the thermographs appear showing average temperatures taken by means of a FLIR T400 IR camera at a frequency of 554.5 MHz for: (a) AUT-coupled SWCNT uncracked bolometer and (b) AUT-coupled SWCNT cracked bolometer. The bolometers were located between the dipolar antenna arms i.e., the antenna feed and each IR image were processed performing the integral of the bolometer temperature pattern.

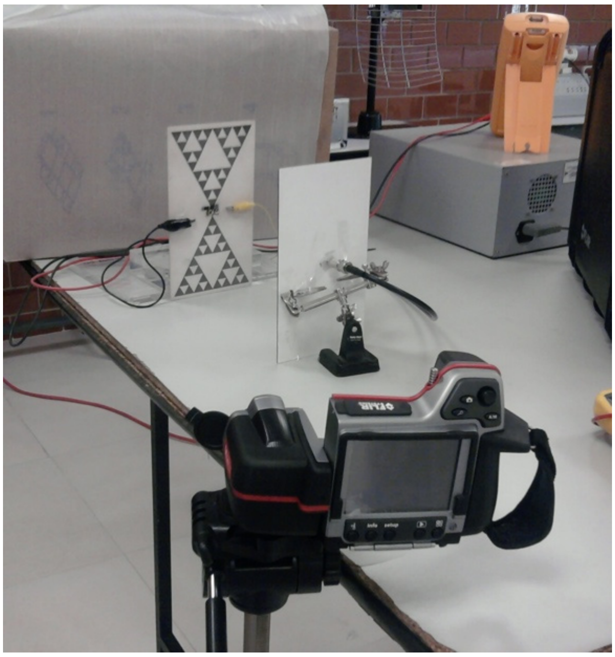

Figure 3. Experimental setup including RFG, TA, AUT, IR camera, and multimeter.

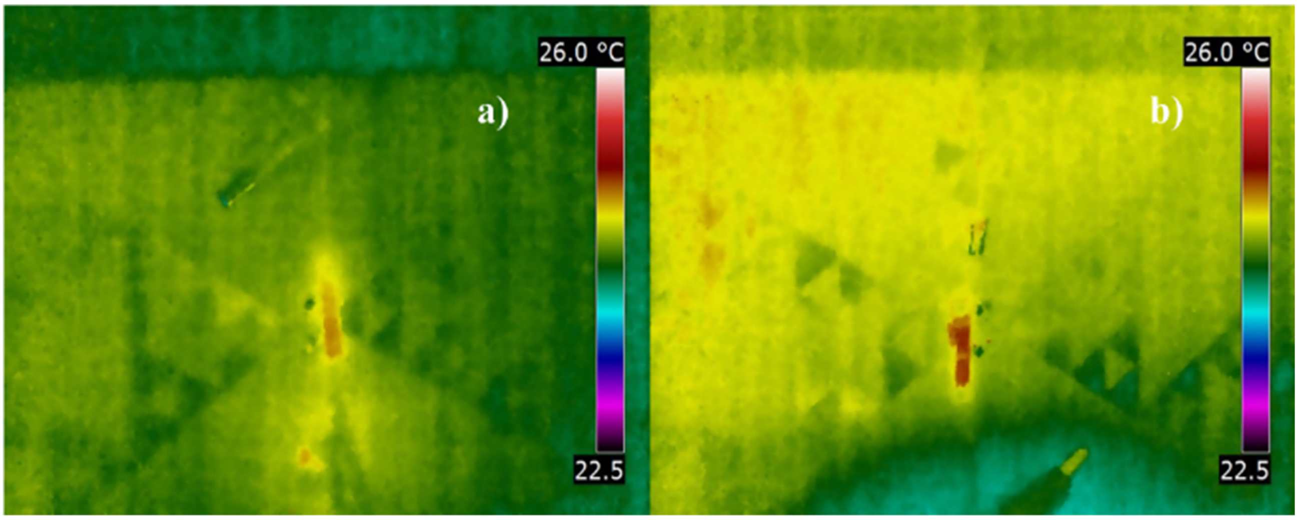

Figure 4. IR thermographs taken at the frequency of 554.5 MHz for: (**a**) AUT-coupled SWCNT uncracked bolometer and (**b**) AUT-coupled SWCNT cracked bolometer. The central red rectangles in (**a**,**b**) correspond to the SWCNT films coupled to the antenna.

3. Results and Discussion

The radiation heat transfer between a surface and the surfaces that surround it is given by Equation (1):

$$\dot{q}_r = \varepsilon\sigma \mathrm{A_s}\left(\mathrm{T}_s^4 - \mathrm{T}_{arround}^4\right) \tag{1}$$

where ε is the emissivity of the surface, σ = 5.67 × 10^{-8} W/m^{2}K is the Stefan-Boltzmann constant, $\mathrm{A_s}$ is the superficial area, T_s is the superficial temperature and $\mathrm{T}_{arround}$ is the surround temperature [37].

The experimental TCR was calculated by the method [38] defined by Equation (2):

$$\mathrm{TCR} = \frac{1}{\mathrm{R}}\frac{\mathrm{dR}}{\mathrm{dT}} \tag{2}$$

where R is the material electrical resistance at T the operation temperature, while the voltage responsivity $\Re_v$ of the bolometer was calculated given by Equation (3) for i_{bias} = 0.1 mA and for an emitted power of 1.5 W [39].

$$\Re v = \frac{i_{bias} \cdot \Delta R}{P_{inc}} \tag{3}$$

Performance of Bolometers

The thermoelectric measurements were performed by monitoring the temperature and electrical resistance of AUT-coupled SWCNT bolometers (cracked and uncracked) as a function of the incident radiation frequency (RFG). The first measurement for the AUT-coupled SWCNT bolometers was conducted feeding the TA at 554.5 MHz, which is the first frequency provided by the RFG. The AUT then experiences electric current flowing through its arms and also a flow by the central part of it (antenna feed), where the bolometer is located. For that reason, the bolometer temperature increased as a result of Joule heating, resulting in a maximum temperature value of 297.81 K for uncracked film, and 298.02 K for cracked film respectively, which decreased the bolometer resistance value to a minimum of 40,283 Ω for uncracked film and 8775 Ω for cracked film also respectively. When tuning the RFG at 678.5 MHz, which was the last frequency available, it occurred the opposite effect, a minimum temperature value of 297.5 K for uncracked film and 297.72 K for cracked film were measured respectively, which increased the bolometer resistance to a maximum value of 40,424 Ω for uncracked film and 8796 Ω for cracked film also respectively, occurring for both films a rise in temperature of SWCNT films upon exposure to radiofrequency radiation which was about 0.31 K. However, the delta resistance (ΔR) is higher in the uncracked sample, which can be seen in Figure 5 and Table 1, where resistance and temperature as a function of the incident frequency are shown.

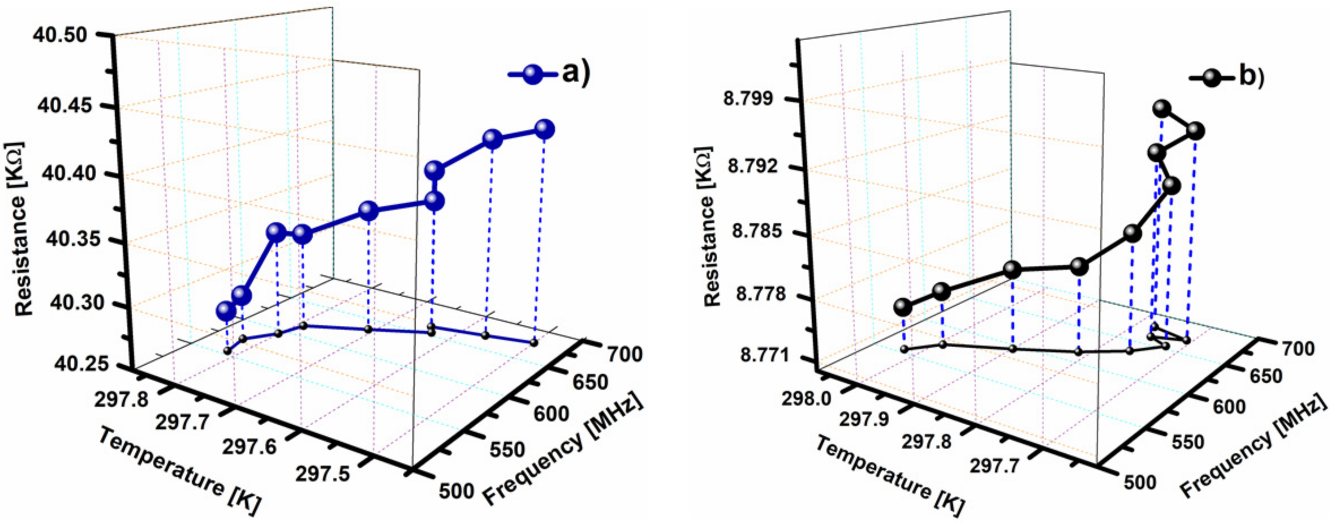

Figure 5. Temperature and resistance of SWCNT as a function of the incident radiation frequency: (**a**) uncracked film and (**b**) cracked film. Both films used as a bolometers coupled to a wideband planar fractal antenna.

Table 1. Measured temperature and resistance in terms of the frequency for uncracked and cracked SWCNT composite films.

		Frequency (MHz)	Temperature (K)	Resistance (KΩ)
Uncracked Sample	Initial measurement	554.5	297.81	40.283
	Final measurement	678.5	297.50	40.424
Cracked Sample	Initial measurement	554.5	298.02	8.775
	Final measurement	678.5	297.72	8.796

Thermo-electrical parameters of the bolometers were obtained: TCR, responsivity, radiation heat, and electric conductivity depending on the sample which was characterized. It is relevant to indicate that, from the original plots (Figure 5), an interpolation on Resistance and Temperature, with 101 points was carried out, to eliminate possible noise peaks, from which a polynomial fit of degree 4 was obtained, substituting the points in each of the Equations (1) and (2). Figure 6 shows TCR for an uncracked film of SWCNT which has an average of $-1.036\%K^{-1}$, with a minimum value of $-3.6\%K^{-1}$ at 297.82 K and a Standard Deviation (SD) of 0.76. In the same figure for the cracked film sample of SWCNT, it shows an average TCR of $-0.55\%K^{-1}$, with a minimum vale of $-1.46\%K^{-1}$ at 298.01 K and SD = 0.54, respectively. It can be observed that the sample of uncracked film of SWCNT exhibits a variability close to 2.5 above the minimum TCR value with respect to the sample of the cracked film of SWCNT, the negative TCR value of the two samples is indicative of semiconductor bolometers, moreover, when metallic SWCNTs are in bundles, as they are in the current work, they exhibit semiconducting behavior due to the interactions between the tubes [40]. Table 2 concentrates thermo-electrical parameters for uncracked and cracked films of SWCNT.

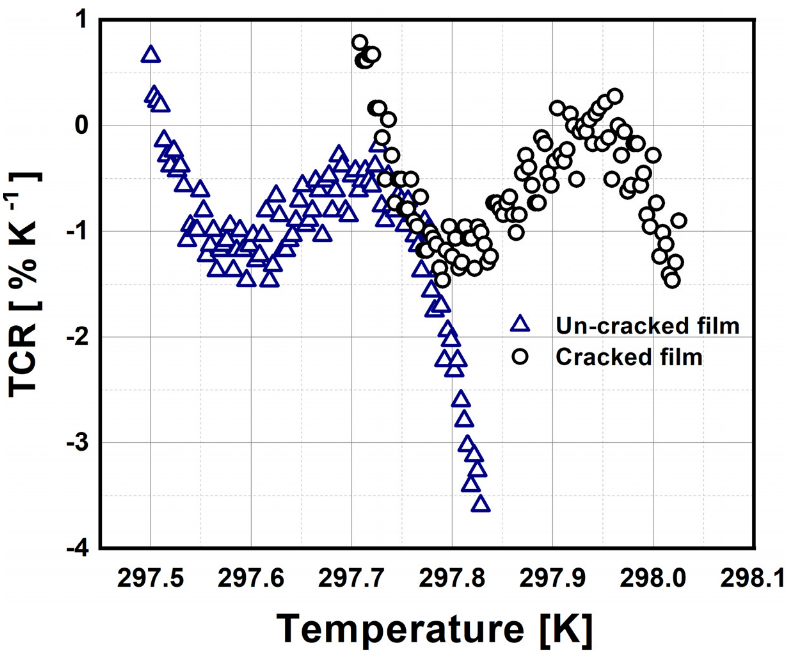

Figure 6. TCR for uncracked and cracked films of SWCNT.

Table 2. Thermo–electrical parameters for uncracked and cracked films of SWCNT.

SWCNT	Minimum Value of TCR ($\%K^{-1}$) ±SD	Temperature at Which TCR is Minimum (K)	Maximum Responsivity (V/W)	Maximum Radiation Heat (μW)	Electric Conductivity (μS m^{-1})
Uncracked	-3.6 ± 0.76	297.82	9.4×10^{-3}	81.7	1.23
Cracked	-1.46 ± 0.5	298.01	1.4×10^{-3}	148.1	5.69

The voltage responsivity was calculated from the experimental results, as shown in Table 1, the uncracked sample has a $\Delta R = 141\ \Omega$ and the cracked sample has a $\Delta R = 21\ \Omega$, which corresponds to values of incident radiation, for the initial frequency of 554.5 MHz and the final frequency of 678.5 MHz, both calculations for an $i_{bias} = 0.1$ mA, dividing these by the incident power [41]. The responsivity value for each cracked and uncracked films are listed in Table 2.

Finally, it is important to mention that if the AUT is in resonance or working near it, as a result of Joule heating, there is a higher temperature concentration in the antenna feed, where the samples were located. The sample with the highest electrical resistance (uncracked film) has an earlier detection of maximum temperature with 297.81 K obtaining from Equation (1) a maximum radiated heat of 81.7 µW, compared to the cracked sample with lower electrical resistance, which detects with a shift of 0.21 K in relation to the sample of uncracked film with the maximum temperature of 298.02 K and with a maximum radiated heat reading of 148.1 µW. It is also important to note that according to $\dot{q}_r$, from Equation (1), the surface temperature is proportional to the emissivity, the Boltzmann constant, and the surface area. Therefore, with a higher temperature value, there will be more radiated heat, which can be seen in Figure 7 and Table 2. The electric conductivity value of these films were 1.23 µS m^{-1} for uncracked and 5.69 µS m^{-1} for cracked sample, respectively.

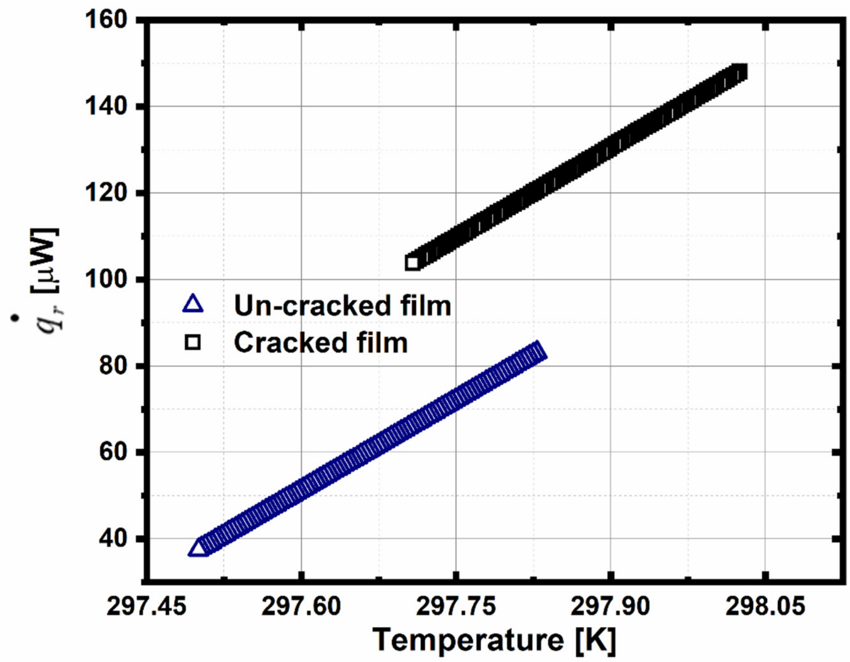

Figure 7. Maximum radiation heat $\dot{q}_r$ as a function of temperature.

4. Conclusions

Results show a significant increase in dissipated heat due to Joule heating at the antenna feed at 554.5 MHz. These results show that it is possible to tune relevant bolometric parameters according to the resonance frequency of interest with which it is required to work, related to each of the iterations of the Sierpinski antenna, as well as the film resistance and TCR by changing the relative humidity of the film. Higher humidity concentrations, i.e., for a relative humidity higher than 80% (uncracked samples) it will result in films with higher electrical resistance, TCR and $\Re_v$, which may be due to greater continuity and alignment of the nanotube throughout the sample, while in the case of cracked films the continuity of the film is reduced as does its electrical resistance, therefore, by decreasing the electrical resistance, there is a greater flow of heat over the sample. This effect is observed in each of the thermal images, in the case of the cracked sample can be seen that there is a higher concentration of temperature in the area where the bolometer is located which is derived from the greater radiated heat, compared to the same area of the uncracked sample. This can be due to the fact that the electrical resistance of the cracked sample is close to five times smaller than the uncracked sample, which makes the cracked sample to be close to five times more conductive than the uncracked sample.

Finally, it is worth mentioning that although the frequency sweep was set from 554.5 MHz to 678.5 MHz, which was the frequency range of the RFG and a range of frequencies between 0-th and 1st AUT iterations, not covering 2nd and 3rd iterations, the bolometric properties of SWCNT bolometers were successfully obtained and demonstrated. A good future work would be to obtain these parameters for AUT-coupled bolometers using an RFG with a wider frequency range to cover 2nd and 3rd iterations and a vector network analyzer to know the impedance behavior.

Author Contributions: Investigation, G.V.-R. and J.S.; conceptualization, G.V.-R. and N.O.-C.; writing-original draft G.V.-R.; supervision G.V.-R., J.S., F.J.G. and J.V.G.-F.; Writing-review & editing, J.S., J.V.G.-F., R.D.d.L.-Z., A.B.d.l.R.-Z. and G.V.-R. validation, J.S., F.J.G., J.F.C.-L. and R.D.d.L.-Z. Software, J.F.C.-L. and A.B.d.l.R.-Z.; formal analysis, F.J.G. and N.O.-C., visualization, J.V.G.-F., methodology. J.F.C.-L. and N.O.-C., project administration, G.V.-R., J.S. and J.V.G.-F. All authors have read and agreed to the published version of the manuscript.

Funding: This research received no external funding.

Acknowledgments: Gustavo Vera Reveles would like to thank José Manuel Gutierrez Hernández for the support in obtaining SEM images. He also thanks Instituto Tecnológico de San Luis Potosí from Tecnológico Nacional de México for the support given in conducting this work and Terahertz Science and Technology National Lab (LANCyTT), Universidad Autónoma de San Luis Potosí, for the support in the use of its thermoelectric measurement infrastructure. It is acknowledged the support from Raymundo V. and Rosa Ma. R. at all moments.

Conflicts of Interest: The authors declare no conflict of interest.

References

1. Li, S.; Yu, Z.; Yen, S.F.; Tang, W.C.; Burke, P.J. Carbon nanotube transistor operation at 2.6 GHz. *Nano Lett.* **2004**, *4*, 753–756. [CrossRef]
2. Rodriguez-Morales, F.; Zannoni, R.; Nicholson, J.; Fischetti, M.; Yngvesson, K.S.; Appenzeller, J. Direct and heterodyne detection of microwaves in a metallic single wall carbon nanotube. *Appl. Phys. Lett.* **2006**, *89*, 083502. [CrossRef]
3. Tarasov, M.; Svensson, J.; Kuzmin, L.; Campbell, E.E.B. Carbon nanotube bolometers. *Appl. Phys. Lett.* **2007**, *90*, 163503. [CrossRef]
4. Fu, K.; Zannoni, R.; Chan, C.; Adams, S.H.; Nicholson, J.; Polizzi, E.; Yngvesson, K.S. Terahertz detection in single wall carbon nanotubes. *Appl. Phys. Lett.* **2008**, *92*, 033105. [CrossRef]
5. Itkis, M.E.; Borondics, F.; Yu, A.; Haddon, R.C. Bolometric infrared photoresponse of suspended single-walled carbon nanotube films. *Science* **2006**, *312*, 413–416. [CrossRef]
6. Lu, R.; Shi, J.J.; Baca, F.J.; Wu, J.Z. High performance multiwall carbon nanotube bolometers. *J. Appl. Phys.* **2010**, *108*, 084305. [CrossRef]
7. Ryger, I.; Lobotka, P.; Steiger, A.; Chromik, S.; Lalinsky, T.; Raida, Z.; Vanko, G. Uncooled Antenna-Coupled Microbolometer for Detection of Terahertz Radiation. *J. Infrared. Milli. Terahz. Waves* **2021**, *42*, 462–478. [CrossRef]
8. García-Valdivieso, G.; Navarro-Contreras, H.R.; Vera-Reveles, G.; González, F.J.; Simmons, T.J.; Hernández, M.G.; Quintana, M.; Nieto Navarro, J.G. High sensitivity bolometers from thymine functionalized multi-walled carbon nanotubes. *Sens. Actuators B Chem.* **2017**, *238*, 880–887. [CrossRef]
9. Kraus, H. Superconductive bolometers and calorimeters. *Supercond. Sci. Technol.* **1996**, *9*, 827–842. [CrossRef]
10. Gonzalez, F.J.; Fumeaux, C.; Alda, J.; Boreman, G.D. Thermal impedance model of electrostatic discharge effects on microbolometers. *Microw. Opt. Technol. Lett.* **2000**, *26*, 291–293. [CrossRef]
11. González, F.J.; Gritz, M.A.; Fumeaux, C.; Boreman, G.D. Two dimensional array of antenna-coupled microbolometers. *Int. J. Infrared Millim. Waves* **2002**, *23*, 785–797. [CrossRef]
12. Kruse, P.W. *Uncooled Thermal Imaging: Arrays, Systems, and Applications*; SPIE Press: Washington, DC, USA, 2001.
13. Chen, C.; Yi, X.; Zhang, J.; Zhao, X. Linear uncooled microbolometer array based on VOx thin films. *Infrared Phys. Technol.* **2001**, *42*, 87–90. [CrossRef]
14. Mottin, E.; Martin, J.-L.; Ouvrier-Buffet, J.-L.; Vilain, M.; Bain, A.; Yon, J.-J.; Tissot, J.-L.; Chatard, J.-P. Enhanced amorphous silicon technology for 320 × 240 microbolometer arrays with a pitch of 35 µm. In Proceedings of the Infrared Technology and Applications XXVII; Andresen, B.F., Fulop, G.F., Strojnik, M., Eds.; SPIE: Orlando, FL, USA, 2001; Volume 4369, p. 250. [CrossRef]

15. Ningyi, Y.; Jinhua, L.; Chan, H.L.W.; Chenglu, L. Comparison of VO2 thin films prepared by inorganic sol-gel and IBED methods. *Appl. Phys. A Mater. Sci. Process.* **2004**, *78*, 777–780. [CrossRef]
16. González, F.J.; Ashley, C.S.; Clem, P.G.; Boreman, G.D. Antenna-coupled microbolometer arrays with aerogel thermal isolation. *Infrared Phys. Technol.* **2004**, *45*, 47–51. [CrossRef]
17. Simón, J.; González, F.J. Nanoantennas for polarisation division multiplexing. *Electron. Lett.* **2011**, *47*, 120–121. [CrossRef]
18. Kopylova, D.S.; Fedorov, F.S.; Alekseeva, A.A.; Gilshteyn, E.P.; Tsapenko, A.P.; Bubis, A.V.; Grebenko, A.K.; Popov, Z.I.; Sorokin, P.B.; Gladush, Y.G.; et al. Holey single-walled carbon nanotubes for ultra-fast broadband bolometers. *Nanoscale* **2018**, *10*, 18665–18671. [CrossRef]
19. Gasper, M.R.; Toonen, R.C.; Hirsch, S.G.; Ivill, M.P.; Richter, H.; Sivarajan, R. Radio Frequency Carbon Nanotube Thin-Film Bolometer. *IEEE Trans. Microw. Theory Tech.* **2017**, *65*, 3278–3284. [CrossRef]
20. Mehdipour, A.; Rosca, I.D.; Sebak, A.; Trueman, C.W.; Hoa, S.V. Full-Composite Fractal Antenna Using Carbon Nanotubes for Multiband Wireless Applications. *IEEE Antennas Wirel. Propag. Lett.* **2010**, *9*, 891–894. [CrossRef]
21. Abbas, S.M.; Sevimli, O.; Heimlich, M.C.; Esselle, K.P.; Kimiaghalam, B.; Foroughi, J.; Safaei, F. Microwave Characterization of Car bon Nanotube Yarns For UWB Medical Wireless Body Area Networks. *IEEE Trans. Microw. Theory Tech.* **2013**, *61*, 3625–3631. [CrossRef]
22. Alonso-Gonzalez, L.; Ver-Hoeye, S.; Fernadez-Garcia, M.; Vazquez-Antuna, C.; Las-Heras Andres, F. On the development of a novel mixed embroidered-woven slot antenna for wireless applications. *IEEE Access* **2019**, *7*, 9476–9489. [CrossRef]
23. Vera-Reveles, G.; Simmons, T.J.; Bravo-Sánchez, M.; Vidal, M.A.; Navarro-Contreras, H.; González, F.J. High-sensitivity bolometers from self-oriented single-walled carbon nanotube composites. *ACS Appl. Mater. Interfaces* **2011**, *3*, 3200–3204. [CrossRef] [PubMed]
24. Simmons, T.J.; Hashim, D.; Vajtai, R.; Ajayan, P.M. Large area-aligned arrays from direct deposition of single-wall carbon nanotube inks. *J. Am. Chem. Soc.* **2007**, *129*, 10088–10089. [CrossRef] [PubMed]
25. Bravo-Sanchez, M.; Simmons, T.J.; Vidal, M.A. Liquid crystal behavior of single wall carbon nanotubes. *Carbon N. Y.* **2010**, *48*, 3531–3542. [CrossRef]
26. Simmons, T.J.; Vera-Reveles, G.; González, G.; Gutiérrez Hernández, J.M.; Linhardt, J.L.; Navarro- Contreras, H.; González, F.J. Bolometric Properties of Semiconducting and Metallic Single-Walled Carbon Nanotube Composite Films. *ACS Photonics* **2015**, *2*, 334–340. [CrossRef]
27. Puente-Baliarda, C.; Romeu, J.; Pous, R.; Cardama, A. On the behavior of the sierpinski multiband fractal antenna. *IEEE Trans. Antennas Propag.* **1998**, *46*, 517–524. [CrossRef]
28. Gerald, E. *Measure, Topology, and Fractal Geometry*, 2nd ed.; Springer: New York, NY, USA, 1990.
29. Puente, C.; Romeu, J.; Pous, R.; Garcia, X.; Benitez, F. Fractal multiband antenna based on the Sierpinski gasket. *Electron. Lett.* **1996**, *32*, 1–2. [CrossRef]
30. Puente, C.; Borja, C.; Navarro, M.; Romeu, J. An iterative model for fractal antennas: Application to the Sierpinski gasket antenna. *IEEE Trans. Antennas Propag.* **2000**, *48*, 713–719. [CrossRef]
31. Kaur, J.; Singh, S.; Kansal, A. Multiband behaviour of sierpinski fractal antenna. *Res. J. Inf. Technol.* **2011**, *3*, 35–43. [CrossRef]
32. Best, S.R. On the significance of self-similar fractal geometry in determining the multiband behavior of the sierpinski gasket antenna. *IEEE Antennas Wirel. Propag. Lett.* **2002**, *1*, 22–25. [CrossRef]
33. Tsachtsiris, G.F.; Soras, C.F.; Karaboikis, M.P.; Makios, V.T. Analysis of a modified Sierpinski gasket monopole antenna printed on dual band wireless devices. *IEEE Trans. Antennas Propag.* **2004**, *52*, 2571–2579. [CrossRef]
34. Kapetanakis, T.N.; Pavec, M.; Ioannidou, M.P.; Nikolopoulos, C.D.; Baklezos, A.T.; Soukup, R.; Vardiambasis, I.O. Embroidered Bow-Tie Wearable Antenna for the 868 and 915 MHz ISM Bands. *Electronics* **2021**, *10*, 1983. [CrossRef]
35. Rogalski, A. *Infrared Detectors*, 2nd ed.; CRC Press: Boca Raton, FL, USA, 2010.
36. Balanis, C.A. *Antenna Theory: Analysis and Design*, 3rd ed.; Wiley: Hoboken, NJ, USA, 2016.
37. Cengel, Y.A. *Heat and Mass Transfer: A Practical Approach*, 3rd ed.; McGraw-Hill: New York, NY, USA, 2006.
38. Rajendra Kumar, R.T.; Karunagaran, B.; Mangalaraj, D.; Narayandass, S.K.; Manoravi, P.; Joseph, M.; Gopal, V. Study of a pulsed laser deposited vanadium oxide based microbolometer array. *Smart Mater. Struct.* **2003**, *12*, 188–192. [CrossRef]
39. Ham, M.H.; Kong, B.S.; Kim, W.J.; Jung, H.T.; Strano, M.S. Unusually large Franz-Keldysh oscillations at ultraviolet wavelengths in single-walled carbon nanotubes. *Phys. Rev. Lett.* **2009**, *102*, 047402. [CrossRef] [PubMed]
40. Ouyang, M.; Huang, J.L.; Cheung, C.L.; Lieber, C.M. Energy gaps in "metallic" single-walled carbon nanotubes. *Science* **2001**, *292*, 702–705. [CrossRef] [PubMed]
41. García, M.; Ambrosio, R.; Torres, A.; Kosarev, A. IR bolometers based on amorphous silicon germanium alloys. *J. Non-Cryst. Solids* **2004**, *338–340*, 744–748. [CrossRef]